Co-design of Power Dispatch with Dynamic Power Regulation and Communication Transmission Optimization for Frequency Control in VPPs

Jinrui Guo, Chunxia Dou, *Fellow*, *IEEE*, Dong Yue, *Fellow*, *IEEE*, Zhijun Zhang, Zhanqiang Zhang, and Bo Zhang

***Abstract*—The increasing integration of intermittent renewable energy sources into distribution networks has exerted significant pressure on the frequency regulation of power systems. Meanwhile, integrating small-capacity battery energy storage systems into distribution network is a growing trend in the construction of virtual power plants (VPPs), which offer great potential advantages in improving the system frequency regulation capabilities. However, the process of power dispatch for VPPs may be hindered by imperfections in the communication network, which affects their frequency control performance. Simultaneously, the economic benefits associated with their frequency control services are often overlooked. As such, we propose a co-design method of power dispatch with dynamic power regulation and communication transmission optimization for frequency control in VPPs. First, a joint design scheme of power dispatch and routing optimization under cloud-edge collaborations is proposed. This scheme encompasses a power dispatch method considering the influences of communication network and a routing optimization policy based on graph convolutional neural networks, both of which are designed to ensure the accurate and real-time frequency control service. Further, we propose a dynamic power regulation strategy under edge-edge collaborations. Specifically, according to the established correction control objective, an adaptive distributed auction algorithm (ADAA) based dynamic power regulation control method is designed to determine the optimal regulation power of VPPs, thereby improving the economic benefits of frequency control service. Finally, the simulation results validate the feasibility and superiority of the proposed co-design method for frequency control.**

***Index Terms*—Virtual power plant (VPP), frequency control, power dispatch, dynamic power regulation, communication transmission optimization, cloud-edge collaboration.**

I. Introduction

UNDER the carbon peaking and carbon neutrality target proposed by China, the penetration rate of renewable energy resources is escalating [1]. Consequently, the proportion of traditional generators is diminishing, leading to a gradual capacity declining in the frequency regulation of power systems [2]. This, in turn, poses a challenge to system frequency stability, necessitating an urgent increase in regulation resources to enhance the frequency security [3]. Besides, the growing integration of distributed resources such as battery energy storage systems (BESSs) into distribution network offers viable options for frequency regulation [4], [5]. However, the sheer number and limited individual capacities of BESSs may exert considerable influences on system operation and management. As a result, the utilization of virtual power plants (VPPs) to aggregate and coordinate BESSs for system frequency control has become an emerging paradigm [6].

Recently, the extensive research has focused on the application of VPPs in frequency control. For example, a hierarchical inertial control strategy for VPPs is developed in [7] to enhance the system frequency response. Reference [8] proposes a bi-level optimal control method for VPPs to participate in the primary frequency regulation market. However, these aforementioned studies fail to explore the capability of VPPs to provide secondary frequency regulation in response to automatic generation control (AGC) signals. In [9], an advanced control technique for VPPs is developed to implement AGC in power systems. To further enhance the response capability of VPPs to AGC, a novel control scheme for sizing VPPs is presented in [10] to mitigate system frequency fluctuations. Additionally, [11] constructs a framework for VPPs to provide AGC services and primary frequency response. Although these studies effectively utilize VPPs for frequency support, few of them have investigated the participation of VPPs in frequency control while considering their economic benefits.

Manuscript received: June 11, 2024; revised: November 18, 2024; accepted: December 2, 2024. Date of CrossCheck: December 2, 2024. Date of online publication: January 20, 2025.

This work was supported in part by the Major Program of the National Natural Science Foundation of China (No. 62293504) and the Postgraduate Research & Practice Innovation Program of Jiangsu Province (No. KYCX24_1212).

J. Guo is with the College of Automation & College of Artificial Intelligence, Nanjing University of Posts and Telecommunications, Nanjing 210023, China, and he is also with the Institute of Advanced Technology for Carbon Neutrality, Nanjing University of Posts and Telecommunications, Nanjing 210023, China (e-mail: 1220055806@njupt.edu.cn).

C. Dou (corresponding author), D. Yue, Z. Zhang, Z. Zhang, and B. Zhang are with the Institute of Advanced Technology for Carbon Neutrality, Nanjing University of Posts and Telecommunications, Nanjing 210023, China, and Z. Zhang is also with the Department of Electrical Engineering, City University of Hong Kong, Hong Kong 999077, China (e-mail: cxdou@ysu. edu. cn; medongy@vip. 163. com; mezhijun@gmail. com; zzq@njupt. edu. cn; zb516869613@163.com).

DOI: 10.35833/MPCE.2024.000604

Furthermore, when VPPs participate in frequency control, they need to communicate with the control center. For this purpose, the wired communication offers notable advantages over wireless communication. Specifically, the wired communication has the benefits of less interference and stronger confidentiality [12]. Thus, this paper adopts wired Ethernet to ensure the real-time performance and reliability requirements of frequency control service. In addition, the communication issues inevitably arise due to the massive measurement information and control instructions of VPPs that need to be transmitted in the frequency control process. Hence, this paper also pays main attention to the influences of communication network. Currently, extensive research has been conducted on the impact of communication network in different scenarios, such as dynamic pricing [13], load control [14], and economic scheduling [15]. In terms of frequency control, [16] investigates the impact of communication delay on inverter air conditioners participating in frequency control. However, few studies have considered the impact of communication network on the frequency control performance of VPPs. Beyond this, the joint design of communication and frequency control in VPPs has not been discussed in existing research.

Besides, considerable literature has been dedicated to exploring the application of cloud-edge frameworks. For instance, a two-stage power regulation method for distribution networks, which leverages the cloud-edge collaboration mechanism, is designed to ensure the system operation stability in [17]. Reference [18] further proposes a power dispatch method based on cloud-edge collaborations, aiming at providing real-time and flexible energy supply. Additionally, [19] introduces a control architecture based on cloud-edge collaborations to address voltage issues in distribution network. Furthermore, a distribution network reconfiguration technique is presented in [20], which achieves voltage preventive control and maintains system safety under the cloud-edge framework. In general, these studies collectively investigate the application of cloud-edge frameworks in economic regulation, voltage control, and topology reconstruction. However, the application of cloud-edge framework to frequency control of VPPs has garnered limited attention.

In light of this, we propose a co-design method of power dispatch with dynamic power regulation and communication transmission optimization under cloud-edge collaborations for frequency control in VPPs. This method aims at supporting the frequency control and ensuring a good frequency response performance. The main contributions of this paper can be summarized as follows.

1) A control architecture based on cloud-edge collaborations is constructed to facilitate the participation of VPPs in frequency control. On this basis, we propose a novel co-design method, which effectively integrates the joint design of power dispatch and routing optimization with dynamic power regulation. To the best of the authors' knowledge, this is the first time such a unified design method is proposed, which leverages VPPs to provide frequency control service.

2) A joint design scheme of power dispatch and routing optimization under cloud-edge collaborations is presented. We propose a power dispatch method considering the influences of communication network. To eliminate these influences, we introduce a routing optimization policy based on graph convolutional neural (GCN) networks. With this scheme, not only the influence of communication network on power dispatch can be mitigated, but also the real-time and accurate frequency control service can be guaranteed.

3) A dynamic power regulation strategy under edge-edge collaborations is proposed. Specifically, to achieve an optimal correction objective, an adaptive distributed auction-based algorithm (ADAA) based dynamic power regulation control method is employed. Through this method, the optimal regulation power of VPPs can be derived, thereby enhancing the economic benefits of frequency control service.

The remainder of this paper is organized as follows. Section II provides the system architecture and method description. Section III presents the joint design scheme of power dispatch and routing optimization under cloud-edge collaborations. The dynamic power regulation strategy under edge-edge collaborations is proposed in Section IV. Simulation results are given in Section V. Finally, Section VI concludes this paper.

II. System Architecture and Method Description

A graphical description of multiple distributed VPPs participating in frequency control under cloud-edge collaborations is displayed in Fig. 1. It mainly includes edge layer, communication layer, and cloud layer.

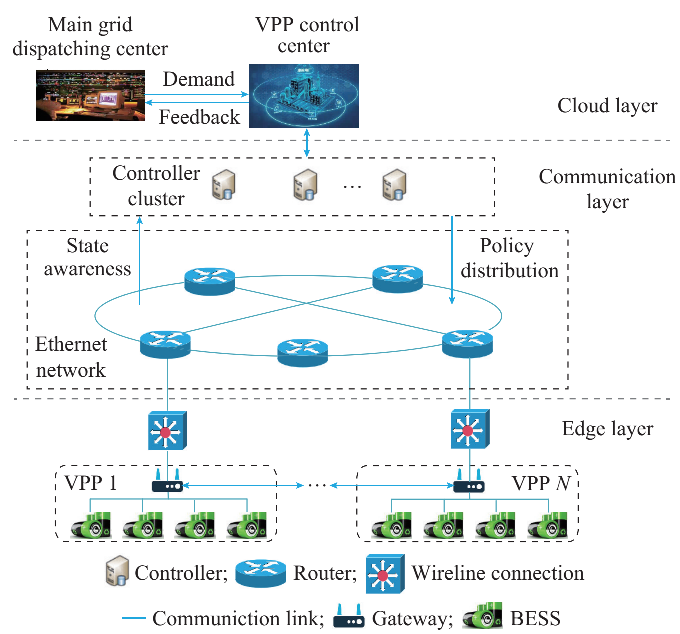

Fig. 1. Graphical description of multiple distributed VPPs participating in frequency control under cloud-edge collaborations.

In the edge layer, numerous aggregation control gateways and BESSs are deployed within the VPPs. These gateways are responsible for gathering information from the BESSs and facilitating interactions with VPP control center and the adjacent VPPs through wireline connections. The communication layer consists of a wired Ethernet network that utilizes software-defined networking (SDN) technology [21]. This technology enables the separation of the network control plane and data plane. Specifically, the control plane within the SDN consists of large-scale controller clusters, whereas the data plane encompasses multiple routers and communication links. These controllers are capable of formulating routing policies and distributing them based on the state awareness of the global network, to fulfill frequency control service demands. Subsequently, the routers receive and forward data and information in accordance with the optimal routing policies. The VPP control center in the cloud layer has the authority to make direct decisions and engages in information exchange with the main grid dispatching center.

This paper focuses on the process of multiple VPPs participating in frequency control. Initially, the VPP control center swiftly allocates AGC instructions received from the main grid dispatching center to each individual VPP, based on their respective regulation capabilities. Subsequently, the local aggregation control gateway of each VPP performs distributed optimization, utilizing the received power regulation instructions, to ascertain its optimal regulation power. Ultimately, the power output of each VPP is adjusted to the optimal value, fulfilling the AGC power regulation task and thereby achieving the frequency control objective. Notably, the power transfer data among VPPs is primarily facilitated through the wired communication technology. In other words, the aggregation control gateway obtains the power regulation variations for a certain VPP through multiple communications with its adjacent VPPs, enabling the regulation of power transfer among them.

Specifically, upon receiving the AGC regulation demand from the main grid dispatching center, the VPP control center first calculates the AGC power regulation task based on the regulation range of VPPs. Subsequently, the VPP control center transmits this allocated AGC power regulation task to the corresponding aggregation control gateway of each VPP through the communication layer. Each aggregation control gateway then interacts with others considering its own adjustment capacity to adjust the power output of VPPs, thereby ensuring the successful completion of the frequency control task. Additionally, given that the distance from the VPP control center to each aggregation control gateway is typically substantial, this paper primarily focuses on the impact of complexity of network environment on frequency control. This complexity can adversely affect the performance of communication, making it challenging to ensure the real-time performance and accuracy of frequency control service. Besides, the AGC power regulation task undertaken by each VPP also fails to enhance the economic benefits of frequency control service.

As such, this paper endeavors to propose a co-design method of power dispatch with dynamic power regulation and communication transmission optimization under cloud-edge collaborations for frequency control in VPPs. As shown in Fig. 2, the framework of the proposed co-design method for frequency control is provided. This framework encompasses a joint design scheme of power dispatch and routing optimization under cloud-edge collaborations, aimed at determining the original allocated power while considering the influences of communication network. Additionally, a dynamic power regulation strategy under edge-edge collaborations is introduced to determine the optimal regulation power of VPPs. By adopting this co-design method, the real-time performance and accuracy of frequency control service can be guaranteed, while its economic benefits can be enhanced simultaneously.

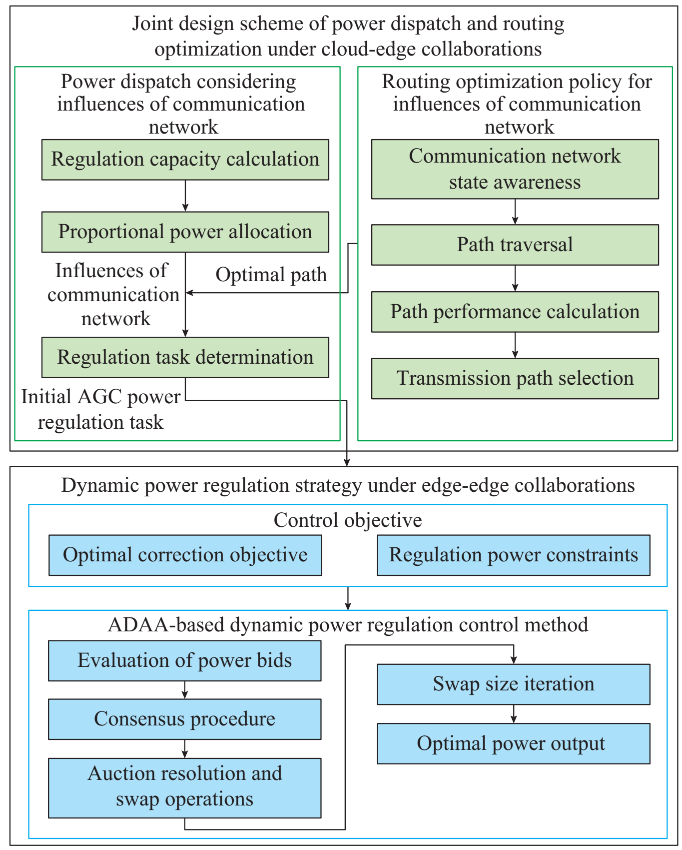

Fig. 2. Framework of proposed co-design method for frequency control.

III. Joint Design Scheme of Power Dispatch and Routing Optimization Under Cloud-Edge Collaborations

In this section, a joint design scheme of power dispatch and routing optimization under cloud-edge collaborations is introduced for the participation of VPPs in frequency control. First, a power dispatch method considering the influences of communication network is proposed to ascertain the AGC power regulation tasks allocated to VPPs. Moreover, to eliminate the influences of communication network, a routing optimization policy based on GCN is designed for selecting the optimal data transmission path.

A. Power Dispatch Method Considering Influences of Communication Network

1) Regulation Capacity Calculation

In the VPP control center, the regulation capacity of VPPs is first considered to guarantee the effective execution of the AGC power regulation tasks from the main grid dispatching center. Thus, the regulation power can be calculated as:

$$\begin{cases} P^{up}(t)=\sum_{i\in\mathcal{N}} P_i^{up}(t) \\ P^{dn}(t)=\sum_{i\in\mathcal{N}} P_i^{dn}(t) \end{cases} \quad \forall t\in\mathcal{T} \tag{1}$$

$$\begin{cases} P_i^{up}(t)=P_i^{\max}(t)-P_i^b(t) \\ P_i^{dn}(t)=-P_i^{\max}(t)-P_i^b(t) \end{cases} \quad \forall i\in\mathcal{N}, t\in\mathcal{T} \tag{2}$$

where $P^{up}(t)$ and $P^{dn}(t)$ are the total up and down regulation power of all VPPs at time t, respectively; $P_i^{up}(t)$ and $P_i^{dn}(t)$ are the up and down regulation power of the i^{th} VPP, respectively; $P_i^{\max}(t)$ is the maximum power output of the i^{th} VPP; $P_i^b(t)$ is the base power output of the i^{th} VPP; and $\mathcal{N}$ and $\mathcal{T}$ are the sets of VPPs and time instants, respectively.

2) Proportional Power Allocation

Based on the regulation capacity of VPPs, the AGC power regulation task undertaken by the VPP control center at time t, denoted as $P^{re}(t)$, can be expressed as:

$$P^{re}(t)=\begin{cases} \min\left(P^{AGC}(t),P^{up}(t)\right) & P^{AGC}(t)>0 \\ \max\left(P^{AGC}(t),P^{dn}(t)\right) & P^{AGC}(t)<0 \end{cases} \tag{3}$$

where $P^{AGC}(t)$ is the required AGC power from the main grid dispatching center.

Then, the AGC power regulation task should be allocated to each VPP [22] and it is proportional to the regulation capacity of each VPP, which can be expressed as:

$$P_{i,id}^{re}(t)=\begin{cases} P^{re}(t)\dfrac{P_i^{up}(t)}{P^{up}(t)} & P^{re}(t)>0, \forall i\in\mathcal{N} \\ P^{re}(t)\dfrac{P_i^{dn}(t)}{P^{dn}(t)} & P^{re}(t)<0, \forall i\in\mathcal{N} \end{cases} \tag{4}$$

where $P_{i,id}^{re}(t)$ is the ideal AGC power regulation task allocated to the i^{th} VPP.

3) Regulation Task Determination Considering Influences of Communication Network

Moreover, during the power dispatch process from the VPP control center to each VPP, the successful completion of the AGC power regulation tasks is highly reliant on the data transmission of the communication layer. However, due to the complexity of network environment, the speed and reliability of data transmission often cannot be fully guaranteed. Therefore, the AGC power regulation tasks can be impacted by the communication network. Here, we primarily focus on the following two types of influences.

1) Influence of network performance: the influence of potential network performance of the transmission path for each VPP on data transmission speed is considered. Thus, this poses a challenge in the real-time performance of frequency control service.

2) Influence of security protection delay: in the frequency control service, there is a certain tolerance for control delay, denoted as $O(t)$, which usually contains path transmission delay $T(t)$, equipment execution delay $E(t)$, and security protection delay $d(t)$. Besides, to ensure the reliable transmission of data, it is necessary to configure security protection mechanism. In this mechanism, the security protection delay often has a predefined lower limit, denoted as $d^0(t)$. Hence, the security protection delay plays a crucial role in ensuring the accuracy of frequency control service and it can be described as:

$$d(t)=\max\left(O(t)-T(t)-E(t),d^0(t)\right) \quad \forall t\in\mathcal{T} \tag{5}$$

Furthermore, to intuitively describe the AGC power regulation task considering the influences of communication network, we utilize the triangular norm operator to fuse the influences of network performance and security protection delay. The fusion variable $Q_i(t)$ is derived as:

$$Q_i(t)=\frac{f_i^{tp}(t)d_i(t)}{1-f_i^{tp}(t)-d_i(t)+2\left(f_i^{tp}(t)+d_i(t)\right)} \quad \forall i\in\mathcal{N} \tag{6}$$

where $f_i^{tp}(t)$ is the network performance value of the transmission path for the i^{th} VPP; and $d_i(t)$ is the security protection delay of the i^{th} VPP.

It should be noted that to establish a consistent measurement standard, it is essential to normalize the two parameters $f_i^{tp}(t)$ and $d_i(t)$ involved in the fusion process.

Finally, we provide the initial AGC power regulation task actually allocated to the i^{th} VPP $P_{0,i}^{re}(t)$ as:

$$P_{0,i}^{re}(t)=F\left(Q_i(t)\right)P_{i,id}^{re}(t) \quad \forall i\in\mathcal{N}, t\in\mathcal{T} \tag{7}$$

$$F\left(Q_i(t)\right)=\frac{w}{\mathrm{e}^{-\alpha Q_i(t)}+\varphi} \quad \forall i\in\mathcal{N}, t\in\mathcal{T} \tag{8}$$

where $F(\cdot)$ is a function of fusion variable $Q_i(t)$; w and φ are the model parameters; and α is the adjustment coefficient.

Note that the influences of communication network can potentially compromise the accuracy and real-time performance of frequency control service. To this end, we propose a routing optimization policy based on GCN for eliminating the influences of communication network.

B. Proposed Routing Optimization Policy for Eliminating Influences of Communication Network

1) Communication Network State Awareness

Using the controllers within SDN, the communication network topology and data information can be acquired. To construct the network topology under investigation, we employ a connected and undirected graph denoted as $\mathcal{G}=(\mathcal{V},\mathcal{E})$, where $\mathcal{V}=\{1,2,\dots,N_0\}$ is the set of all nodes, and N_0 is the number of network nodes; and $\mathcal{E}$ is the set of all communication links in the network. Furthermore, the collected network information includes packet loss rate, throughput, and time delay.

2) Path Traversal

As in [23], we adopt the depth-first search algorithm to find all paths between the source node (i.e., VPP control center) and destination nodes (i. e., VPPs). As this is not the main focus of our study, the relevant process is not described here. More details can be referred to [23].

3) Path Performance Calculation

Based on the obtained set of paths, a GCN-based performance prediction method is used to determine the network performance associated with these paths. The overall steps of this method include the following.

Step 1: acquisition of network performance labels for nodes. Given that the collected historical network information encompasses diverse features and exhibits significant variations across different network environments, it poses challenges for training network models. Consequently, we employ the K-means algorithm to cluster the collected data, thereby obtaining network performance labels for the nodes. Furthermore, to ascertain the optimal number of clusters, we introduce the Calinski-Harabasz metric [24] to assess the clustering effectiveness. Additionally, the network features within distinct clustering classes are not directly comparable, so it is imperative to develop a comprehensive metric to evaluate which cluster exhibits superior network performance. To this end, we utilize a multi-metric evaluation approach [25] and the weighted average method to formulate the comprehensive metric, which is illustrated as:

$$f_i^{np}=\sum_{j\in\mathcal{M}}\alpha_j x_{ij}\quad \forall i\in\mathcal{V} \tag{9}$$

where f_i^{np} is the network performance value of the i^{th} node; $\mathcal{M}=\{1,2,\dots,M\}$ is the set of network features, and M is the number of network features; α_j is the weight allocated to feature j; and x_{ij} is the normalized network feature.

Step 2: node classification. According to the obtained node features as well as their corresponding clustering classes and network performance, the supervised training of the GCN model is conducted for node classification.

In this work, we primarily consider the following two basic aspects as inputs of the GCN model.

1) The node feature matrix $\boldsymbol{X}\in\mathbf{R}^{N_0\times M}$, which encapsulates information on network features including packet loss rate L_i, throughput T_i, and time delay D_i (so we have $\boldsymbol{X}=\left[\boldsymbol{x}_1,\boldsymbol{x}_2,\dots,\boldsymbol{x}_{N_0}\right]^{\mathrm{T}}$ and $\boldsymbol{x}_i=\left[L_i,T_i,D_i\right]^{\mathrm{T}}$, $\forall i\in\mathcal{V}$).

2) The adjacency matrix $\boldsymbol{A}=\left[A_{ij}\right]\in\mathbf{R}^{N_0\times N_0}$, which represents the topological connectivity of the communication network. Specifically, if nodes i and j ($i,j\in\mathcal{V}$) are connected, $A_{ij}=1$ ($A_{ij}=A_{ji}$ for undirected networks when $i\neq j$); otherwise, $A_{ij}=0$.

Furthermore, we utilize a layer-wise propagation rule based on the node feature matrix $\boldsymbol{X}$ and adjacency matrix $\boldsymbol{A}$ to obtain the output of GCN model, which is expressed as:

$$\boldsymbol{H}^{(l+1)}=\sigma\left(\tilde{\boldsymbol{D}}^{-\frac{1}{2}}\tilde{\boldsymbol{A}}\tilde{\boldsymbol{D}}^{-\frac{1}{2}}\boldsymbol{H}^{(l)}\boldsymbol{W}^{(l)}\right)=\sigma\left(\hat{\boldsymbol{A}}\boldsymbol{H}^{(l)}\boldsymbol{W}^{(l)}\right) \tag{10}$$

where $\boldsymbol{H}^{(l)}$ is the node feature matrix of the l^{th} layer; σ is the ReLU activation function; $\tilde{\boldsymbol{A}}=\boldsymbol{A}+\boldsymbol{I}$ is the adjacency matrix with self-loops, and $\boldsymbol{I}$ is the identity matrix; $\hat{\boldsymbol{A}}=\tilde{\boldsymbol{D}}^{-\frac{1}{2}}\tilde{\boldsymbol{A}}\tilde{\boldsymbol{D}}^{-\frac{1}{2}}$ is the self-normalized adjacency matrix, and $\tilde{\boldsymbol{D}}$ is the degree matrix; and $\boldsymbol{W}^{(l)}$ is the trainable weight matrix of the l^{th} layer.

Here, we design a two-layer GCN model to predict the network performance of each node. Consequently, the final outputs $\boldsymbol{Z}$ can be expressed as:

$$\boldsymbol{Z}=\operatorname{softmax}\left(\hat{\boldsymbol{A}}\sigma\left(\hat{\boldsymbol{A}}\boldsymbol{X}\boldsymbol{W}^{(0)}\right)\boldsymbol{W}^{(1)}\right) \tag{11}$$

Subsequently, we utilize the cross-entropy loss function to train the network model, which can be expressed as:

$$L=-\frac{1}{\left|\mathcal{N}_{tr}\right|}\sum_{i\in\mathcal{N}_{tr}}\sum_{j\in\mathcal{M}_c}y_{ij}\lg\hat{y}_{ij} \tag{12}$$

where $\mathcal{N}_{tr}$ and $\mathcal{M}_c$ are the sets of training labels and network class labels, respectively; and y_{ij} and $\hat{y}_{ij}$ are the true label and predicted probability value for the i^{th} node, respectively.

Additionally, to minimize the loss function efficiently, the Adam optimizer is adopted for the high learning efficiency and fast convergence speed.

Step 3: performance calculation. Here, let $\mathcal{P}_i$ denote the set of paths for the i^{th} VPP, where each path comprises multiple nodes. Subsequently, by inputting these node features into the pre-trained model, we can obtain the label of each node. Thus, based on the network performance value allocated to each node, we obtain f_i^{tp} as:

$$f_i^{tp}=\sum_{l\in p}f_l^{np}\quad p\in\mathcal{P}_i,i\in\mathcal{N} \tag{13}$$

where $l\in p$ represents the l^{th} node connected to the p^{th} path.

4) Transmission Path Selection

To mitigate the influence of communication network on frequency control service, it is imperative to select an optimal data transmission path that ensures the actual AGC power regulation task closely align with the ideal one. Besides, in the frequency control service, it is essential to maximize the accuracy while simultaneously meeting the real-time requirements of the control operation.

According to the aforementioned analysis, a transmission path needs to be selected from the following two perspectives.

In terms of network performance, the path must first satisfy the predefined minimum requirement f_0^{tp}, which can be expressed as:

$$f_p^{tp}>f_0^{tp}\quad p\in\mathcal{P}_i,i\in\mathcal{N} \tag{14}$$

For the i^{th} VPP, the network performance of all paths within the set $\mathcal{P}_i$ can be calculated according to (13). On this basis, the objective is to maximize the security protection delay d_p as much as possible:

$$\max d_p\quad p\in\mathcal{P}_i,i\in\mathcal{N} \tag{15}$$

Here, we assume that the tolerances of control delay and equipment execution delay are constant, as indicated by (5). Consequently, to achieve the above objective, we only need to guarantee that the path transmission delay is minimized. In other words, we can further formulate (15) as:

$$\min T_p\quad p\in\mathcal{P}_i,i\in\mathcal{N} \tag{16}$$

where T_p is the path transmission delay of the p^{th} path.

In conclusion, the mathematical model for transmission path selection can be described as:

$$\begin{cases} p^*=\underset{p\in\mathcal{P}_i,i\in\mathcal{N}}{\arg\min}\,T_p \\ \text{s.t. } T_p=\sum_{l\in p}D_l \\ \qquad f_p^{tp}=\sum_{l\in p}f_l^{np} \\ \qquad f_p^{tp}>f_0^{tp} \end{cases} \tag{17}$$

where D_l is the time delay of the l^{th} node in this path.

Thus, based on the path selection model, we can obtain an optimal path p^* that exhibits the highest network performance and the minimum transmission delay, serving as the data transmission path.

IV. Dynamic Power Regulation Strategy Under Edge-edge Collaborations

In this section, a dynamic power regulation strategy under edge-edge collaborations is developed for responding to the AGC power regulation tasks emanating from the VPP control center. Its main objective is to maximize the economic benefits of the frequency control service. Then, we propose an ADAA-based dynamic power regulation control method, which is designed to ascertain the optimal regulation power for all VPPs.

A. Control Objective

The primary objective of this paper is to guarantee that all VPPs are seamlessly coordinated to provide the optimal response performance to AGC power regulation tasks at each time instant t. This is crucial because the initial AGC power regulation task allocated to the VPPs by the VPP control center may not necessarily guarantee the lowest total frequency control cost. Thus, we compare the total frequency control cost caused by regulation power after correction with the cost associated with the initial AGC power regulation task. Then, the correction objective is expressed as:

$$\min \Phi(t) = \sum_{i \in \mathcal{N}} \left(\varphi_i(t) - \varphi_i^0(t) \right) \quad \forall t \in \mathcal{T} \tag{18}$$

$$\varphi_i(t) = \varphi_i^{oc}(t) + \varphi_i^{lc}(t) \quad \forall i \in \mathcal{N}, t \in \mathcal{T} \tag{19}$$

$$\varphi_i^{oc}(t) = a_i \left(P_i^{re}(t) \right)^2 + b_i P_i^{re}(t) + c_i \quad \forall i \in \mathcal{N}, t \in \mathcal{T} \tag{20}$$

$$\varphi_i^{lc}(t) = c_a P_i^{re}(t) \quad \forall i \in \mathcal{N}, t \in \mathcal{T} \tag{21}$$

where $\Phi(t)$ is the overall objective function for the participation of VPPs in frequency control; $P_i^{re}(t)$ is the regulation power of the i^{th} VPP after correction; $\varphi_i(t)$ and $\varphi_i^0(t)$ are the total frequency control costs incurred by regulation power after correction and the initial AGC power regulation task, respectively; $\varphi_i^{oc}(t)$ and $\varphi_i^{lc}(t)$ are the operation cost and loss cost of the i^{th} VPP, respectively; a_i, b_i and c_i are the coefficients of operation cost for the i^{th} VPP; and c_a is the discount coefficient for loss cost [8]. Given the similarity in the expression of $\varphi_i^0(t)$ to that of $\varphi_i(t)$, it is omitted here.

In the process of dynamic regulation, the total regulation power of VPPs after correction is required to satisfy the total AGC power regulation tasks, i.e.,

$$\sum_{i \in \mathcal{N}} P_i^{re}(t) = \sum_{i \in \mathcal{N}} P_{0,i}^{re}(t) \quad \forall t \in \mathcal{T} \tag{22}$$

In addition, the power regulation of each VPP is constrained by its regulation capability, ensuring that the regulation power does not exceed the permitted regulation power limits:

$$P_{i,\min}^{re}(t) \le P_i^{re}(t) \le P_{i,\max}^{re}(t) \quad \forall i \in \mathcal{N}, t \in \mathcal{T} \tag{23}$$

where $P_{i,\min}^{re}(t)$ and $P_{i,\max}^{re}(t)$ are the lower and upper limits of regulation power for the i^{th} VPP, respectively.

B. ADAA-based Dynamic Power Regulation Control Method

The ADAA is modified from an auction-based algorithm, which is inspired by double-sided auctions [26], [27]. Among them, each VPP can be deemed as an agent capable of progressively updating its regulation power through interactions with adjacent agents. To model the interaction network among these diverse agents, we employ an undirected graph $\mathcal{G} = \left(\mathcal{B}, \mathcal{C}, \boldsymbol{\mathcal{A}} \right)$, where $\mathcal{B} = \left\{ b_1, b_2, \ldots, b_N \right\}$ is the set of agents; $\mathcal{C}$ denotes the interactions between agents; and $\boldsymbol{\mathcal{A}}$ is a weighted adjacency matrix, in which each element $\mathcal{A}_{ij}$ represents the connectivity between agents. Specifically, if there is a connection between agents i and j $\left(i,j \in \mathcal{B} \right)$, $\mathcal{A}_{ij} = 1$; otherwise, $\mathcal{A}_{ij} = 0$. Hence, for any given agent i, the set of its adjacent agents $\varXi_i$ can be defined as:

$$\varXi_i = \left\{ b_j \in \mathcal{B} | \mathcal{A}_{ij} = 1, j \ne i \right\} \quad \forall i \in \mathcal{N} \tag{24}$$

On this basis, we mainly describe the following four operations to find the optimal regulation power after correction.

1) Evaluation of Power Bids

Since each VPP is capable of functioning as either a buyer or a seller, the corresponding target variation is calculated based on power bids as:

$$\begin{cases} \beta_i = f_i\left(P_i^{re} + \Delta P_i \right) - f_i\left(P_i^{re} \right) & \text{VPP is a buyer}, \forall i \in \mathcal{N} \\ \gamma_i = f_i\left(P_i^{re} \right) - f_i\left(P_i^{re} - \Delta P_i \right) & \text{VPP is a seller}, \forall i \in \mathcal{N} \end{cases} \tag{25}$$

$$f_i(t) = \varphi_i(t) - \varphi_i^0(t) \quad \forall i \in \mathcal{N}, t \in \mathcal{T} \tag{26}$$

where $f_i(t)$ is the objective function of the i^{th} VPP; $\Delta P_i > 0$ is the swap size of the i^{th} VPP; and β_i and γ_i are the objective increment and decrement of the i^{th} VPP, respectively.

2) Consensus Procedure

The increment in regulation power of each VPP should be balanced through one of its adjacent VPPs. Specifically, when the regulation power of a VPP increases by ΔP_i, the regulation power of one of its adjacent VPPs is required to decrease by the same amount. Thus, the reduction in objective value λ_{ij} can be expressed as:

$$\lambda_{ij} = \gamma_j - \beta_i \quad \forall i,j \in \mathcal{N}, i \ne j \tag{27}$$

Given that each VPP can only engage in power trading with one of its adjacent VPPs, it is necessary to select the optimal one from the adjacent VPPs. To minimize the objective value, we choose the adjacent VPP that causes the maximum reduction in the objective value, which can be formulated as:

$$\lambda_i^{\max} = \max_{j \in \varXi_i} \lambda_{ij} \quad \forall i \in \mathcal{N} \tag{28}$$

$$\rho_i = \arg \max_{j \in \varXi_i} \lambda_{ij} \quad \forall i \in \mathcal{N} \tag{29}$$

where $\lambda_i^{\max}$ is the maximum reduction in objective deviation caused by power bidding; and ρ_i is the index of the optimal adjacent VPP for the i^{th} VPP.

3) Auction Resolution and Swap Operations

When the i^{th} VPP achieves a greater reduction in the objective value compared with its adjacent VPPs, the auction resolution based on the current value of $\lambda_i^{\max}$ will be determined. This can be mathematically expressed as:

$$\lambda_i^{\max} > \max_{j \in \varXi_i} \lambda_j^{\max} \quad \forall i \in \mathcal{N} \tag{30}$$

$$\lambda_i^{\max} > 0 \quad \forall i \in \mathcal{N} \tag{31}$$

If the above constraints are satisfied, the regulation power of the i^{th} VPP and its optimal adjacent VPP will subsequently be updated, as expressed by:

$$P_i^{re}(k+1) = P_i^{re}(k) + \Delta P_i(k) \quad \forall i \in \mathcal{N} \tag{32}$$

$$P_{\rho_i}^{re}(k+1) = P_{\rho_i}^{re}(k) - \Delta P_i(k) \quad \forall i \in \mathcal{N} \tag{33}$$

where k is the iteration number.

4) Swap Size Iteration

Given that each VPP needs to compute the reduction in objective value and transmit the result to its adjacent VPPs, the significant computational complexity cannot be avioded within the algorithm. As such, an adaptive swap size based solution is utilized, which dynamically adjusts the exchange power based on the optimization results. Thus, the swap size of the i^{th} VPP can be written as:

$$\Delta P_i(k+1) = \begin{cases} \theta \Delta P_i(k) & \lambda_i^{\max} > 0, \forall i \in \mathcal{N} \\ \Delta P_i(k)/\theta & \text{else} \end{cases} \tag{34}$$

where θ is the gain factor with the condition of $\theta > 1$.

Furthermore, to ensure compliance with the power balance constraint outlined in (22), the total initial regulation power allocated to VPPs is supposed to be equal to the total AGC power regulation tasks. Therefore, the initial regulation power allocated to each VPP is proportional to its adjustment capability, which can be given as:

$$P_i^{re}(k=1) = \sum_{i \in \mathcal{N}} P_{0,i}^{re} \frac{P_{i,\max}^{re} - P_{i,\min}^{re}}{\sum_{j \in \mathcal{N}} \left(P_{j,\max}^{re} - P_{j,\min}^{re} \right)} \quad \forall i \in \mathcal{N} \tag{35}$$

Additionally, the updated regulation power of each VPP should adhere to the power regulation constraint in (23), which can be expressed as:

$$P_i^{re}(k) = \begin{cases} P_{i,\min}^{re} & P_i^{re}(k) < P_{i,\min}^{re}, \forall i \in \mathcal{N} \\ P_{i,\max}^{re} & P_i^{re}(k) > P_{i,\max}^{re}, \forall i \in \mathcal{N} \end{cases} \tag{36}$$

In conclusion, a comprehensive description of the proposed dynamic power regulation control method is illustrated in Algorithm 1. Based on this method, the AGC power regulation tasks emanating from the VPP control center can be fulfilled in an optimal manner by using the cooperation of multiple VPPs.

Algorithm 1: proposed dynamic power regulation control method

1. **Input**: the AGC power regulation task $P_{0,i}^{re}$ of the i^{th} VPP
2. Set $k=1$ and initialize the number of VPPs N, the interaction network, the maximum iteration number $k^{\max}$, the swap size ΔP_i, and the gain factor θ
3. Acquire the regulation capabilities of all VPPs
4. Calculate initial regulation power allocated to the i^{th} VPP based on (35)
5. **Repeat**
6. $k = k+1$
7. **for** $i = 1, 2, ..., N$ **do**
8. Implement the objective variations β_i and γ_i based on (25) and (26)
9. Perform the consensus procedure based on (27)-(29)
10. Find the auction resolution and update the regulation power of the i^{th} VPP based on (30)-(33)
11. Limit the updated regulation power of the i^{th} VPP based on (36)
12. Update the swap size of the i^{th} VPP based on (34)
13. **end**
14. **until** $k = k^{\max}$
15. **Output**: the optimal regulation power to all VPPs

Remark 1: according to [24], the convergence of the proposed ADAA can be proven via mimicking the convergence proof of pattern search algorithms and more details can be referred to [24].

V. Simulation Results

To verify the effectiveness of the proposed co-design method for frequency control, we implement extensive simulations in this section. As shown in Fig. 3(a), a test region with a 30-node communication network topology is adopted for simulation verification. Among these nodes, black node 1 and red nodes 8, 13, 23, 26, and 29 are selected as the network access points for the VPP control center and VPPs to facilitate information interaction, respectively. Furthermore, we divide the dataset containing 30000 network features into training, validation, and testing sets in a ratio of 8:1:1 to train a GCN model. In this model, we set the training epoch to be 400 and the learning rate to be 0.001. In addition, the interaction network of all VPPs is shown in Fig. 3(b). The basic parameters of simulation are set as follows: $w=1$, $\varphi=1$, $\alpha=20$, $k^{\max}=50$, and $\theta=2$.

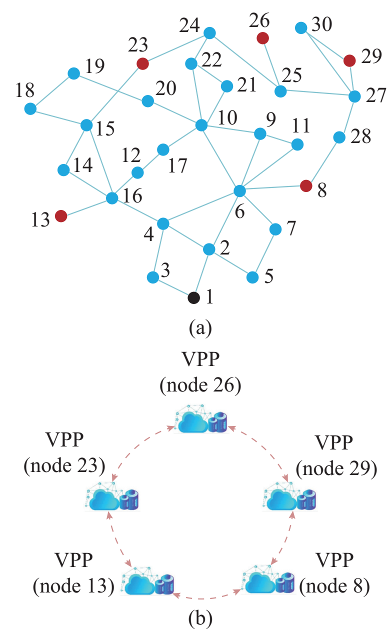

Fig. 3. Test system. (a) 30-node communication network topology. (b) Interaction network of all VPPs.

A. Validity of Joint Design Scheme of Power Dispatch and Routing Optimization Under Cloud-edge Collaborations

1) Validity of Proposed Routing Optimization Policy

In this case study, we analyze the effectiveness of the proposed routing optimization policy in terms of model prediction performance evaluation and comparison with some existing policies.

1) Model prediction performance evaluation

To investigate the model prediction performance, it is necessary to determine the number of network performance labels. As such, in our experiment, the Calinski-Harabasz results are investigated across a range of clustering numbers (from 2 to 10 with an interval of 1), as shown in Fig. 4. We can find that the highest Calinski-Harabasz value occurs with 4 clustering classes, indicating that the optimal number of clustering classes is 4. In other words, the best clustering performance is achieved. Thus, in this study, the number of network performance labels is set to be 4, denoted as C1, C2, C3, and C4 for convenience.

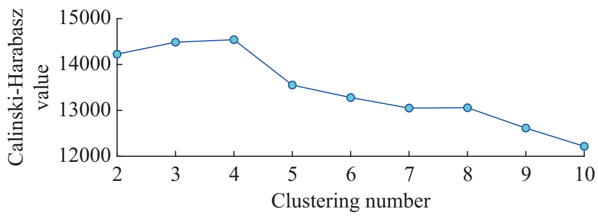

Fig. 4. Calinski-Harabasz results with different clustering numbers.

Then, leveraging the feature information and network performance labels of nodes, the training of the proposed GCN model is executed. We can observe from Fig. 5 that both the training and validation accuracies exhibit a rapid increase, while the training and validation loss values decrease progressively as the number of epochs increases. Meanwhile, when the training reaches 300 epochs, these curves tend to level off. The above results confirm the effectiveness of the proposed GCN model and indicate that this model exhibits good performance and generalization capabilities. To further evaluate the node classification ability of the proposed GCN model, the testing set is fed into the trained model. As shown in Fig. 6, the node classification results illustrated by the confusion matrix reveal the detailed performance insights. The node classification performance for each label is provided in Table I, utilizing various common metrics such as accuracy, precision, recall, and F1-score [28]. The average accuracy, precision, recall, and F1-score are 99.483%, 98.917%, 98.920%, and 98.919%, respectively, suggesting that the proposed GCN model has excellent node classification performance.

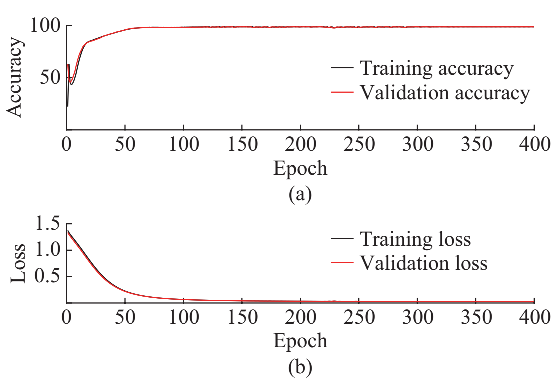

Fig. 5. Training and validation results of proposed GCN model. (a) Training and validation accuracies. (b) Training and validation losses.

Further, to validate the superiority of the proposed GCN model in node label prediction, we compare it with four benchmark models on the same dataset, including decision tree (DT) [29], fully connected network (FCN) [30], support vector machine (SVM) [31], and convolutional neural network (CNN) [32]. Figure 7 displays the performance comparison results of these models for node classification. We can observe from Fig. 7 that the proposed GCN model outperforms all benchmark models in prediction. For instance, while all models achieve an accuracy of over 90%, the proposed GCN model demonstrates a higher node classification accuracy compared with others. Additionally, Fig. 8 visually demonstrates the confusion matrix of different models for node classification. Through these experimental verifications and analyses, it is evident that the proposed GCN model is a promising approach for node label prediction.

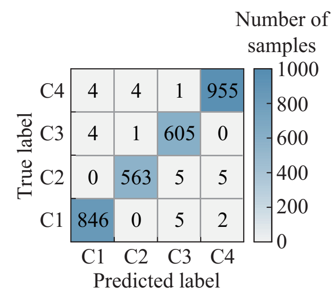

Fig. 6. Confusion matrix of proposed GCN model for node classification.

TABLE I
NODE CLASSIFICATION PERFORMANCE FOR EACH LABEL

Label	Accuracy (%)	Precision (%)	Recall (%)	F1-score (%)
C1	99.500	99.063	99.179	99.121
C2	99.500	99.120	98.255	98.685
C3	99.467	98.214	99.180	98.695
C4	99.467	99.272	99.066	99.169

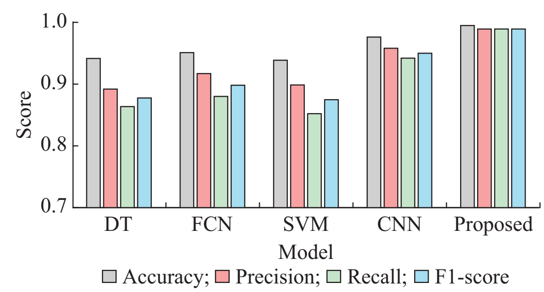

Fig. 7. Performance comparison results of different models for node classification.

2) Comparison of proposed routing optimization policy with existing policies

To validate the effectiveness of the proposed routing optimization policy, we compare it with two benchmark policies: the hop-based routing (HBR) [33] and the Dijkstra-based routing (DBR) policies [34]. The comparison results in terms of the packet loss rate, throughput, time delay, and network performance of each VPP are illustrated in Fig. 9.

From Fig. 9, we can observe that although the DBR policy has a slight advantage in terms of packet loss rate compared with the proposed routing optimization policy, it exhibits significant deficiencies in other aspects. In addition, despite the HBR and proposed routing optimization policies demonstrate similar performance in terms of packet loss rate, throughput, and network performance, the HBR cannot effectively alleviate time delay. The advantage of the proposed routing optimization policy lies in that it can fully consider network performance and dynamically select the optimal path with the minimum transmission delay.

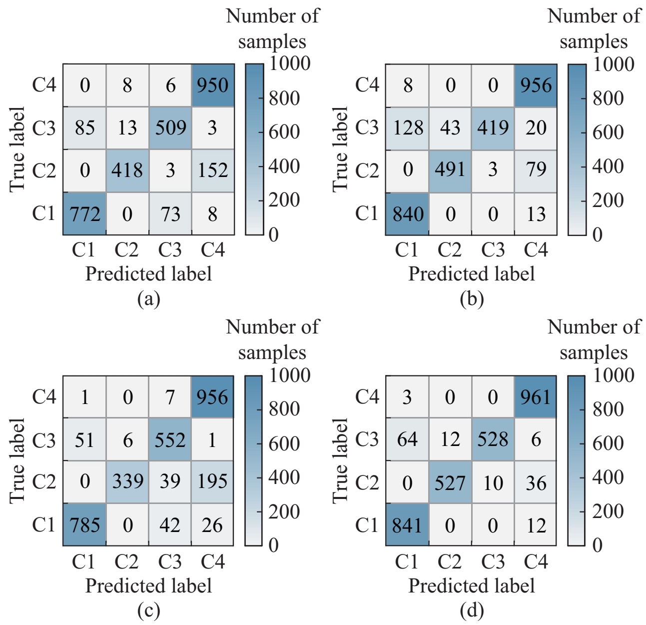

Fig. 8. Confusion matrix of different models for node classification. (a) DT. (b) FCN. (c) SVM. (d) CNN.

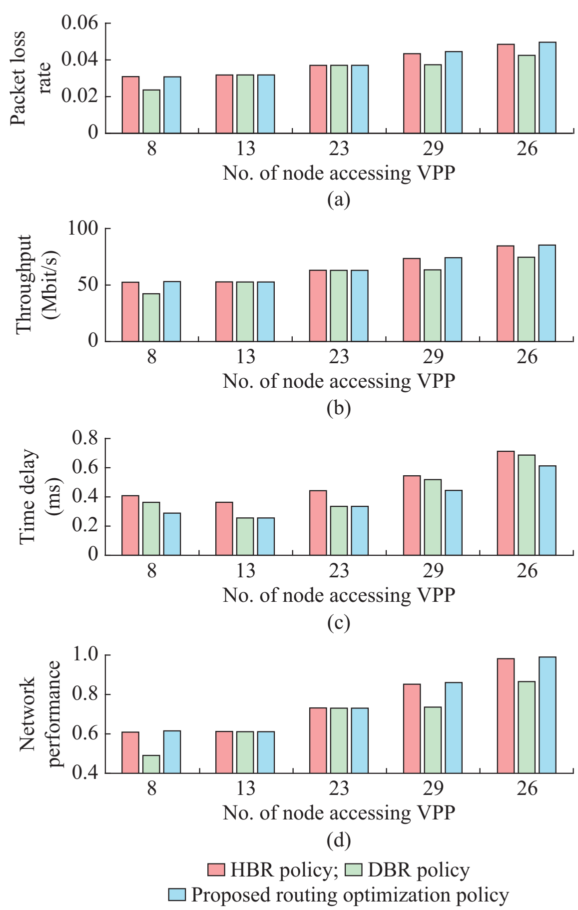

Fig. 9. Comparison results of each VPP. (a) Packet loss rate. (b) Throughput. (c) Time delay. (d) Network performance.

In contrast, the benchmark policies solely focus on selecting the shortest distance or smallest hop-count path, neglecting both network performance and the minimum time delay.

Table II gives the average results of different policies in terms of the packet loss rate, throughput, time delay, and network performance. We can find from Table II that although the packet loss rate of the proposed routing optimization policy is 12.46% higher than that of the DBR policy, it surpasses the comparison policies in other aspects. Specifically, compared with the HBR and DBR policies, the proposed routing optimization policy reduces time delay by 21.61% and 10.28%, respectively, and enhances network performance by 0.55% and 10.89%. As a result, the effectiveness of the proposed routing optimization policy in eliminating influences of communication network can be guaranteed by the simulation results.

TABLE II
AVERAGE RESULTS OF DIFFERENT POLICIES

Policy	Packet loss rate	Throughput (Mbit/s)	Time delay (ms)	Network performance
HBR	0.0383	65.2918	0.4943	0.7573
DBR	0.0345	59.2076	0.4319	0.6867
Proposed	0.0388	65.6587	0.3875	0.7615

2) Validity of Power Dispatch Considering Influences of Communication Network

In this case study, we analyze the validity of the proposed power dispatch method by comparing it with some benchmark methods, which are: ① Method 1, which performs a proportional power allocation approach from [35] without considering the impact of communication network; ② Method 2, which adopts the scheme of Method 1 but incorporates the proposed routing optimization policy. Figures 10 compares the AGC regulation power and VPP power output and Fig. 11 illustrates the total cost of VPP with different methods. A detailed performance comparison among these methods is further provided in Table III.

As illustrated in Fig. 10, we can observe that the proposed power dispatch method exhibits superior frequency response performance.

In addition, we can see from Table III that compared with Method 1, the proposed power dispatch method reduces the average power deviation by 93.33% and the maximum power deviation by 10.46%. This is because the influences of communication network on frequency control can be eliminated with the proposed routing optimization policy, resulting in a reduction in power deviation. As a result, the proposed co-design method for frequency control can enhance the accuracy and real-time performance of the frequency control service in VPPs.

As illustrated in Fig. 11 and Table III, we can observe that although Method 1 has a lower average total cost, it exhibits poor frequency response performance. This is due to the influences of communication network on the accuracy of the AGC power regulation tasks received by VPPs. Both of the proposed power dispatch method and Method 2 can effectively minimize the error between ideal and actual AGC regulation power. However, Method 2 has a low cost efficiency. Thus, the proposed co-design method for frequency control can guarantee a good frequency response performance while improving the economic benefits of the frequency control service through the simulation results.

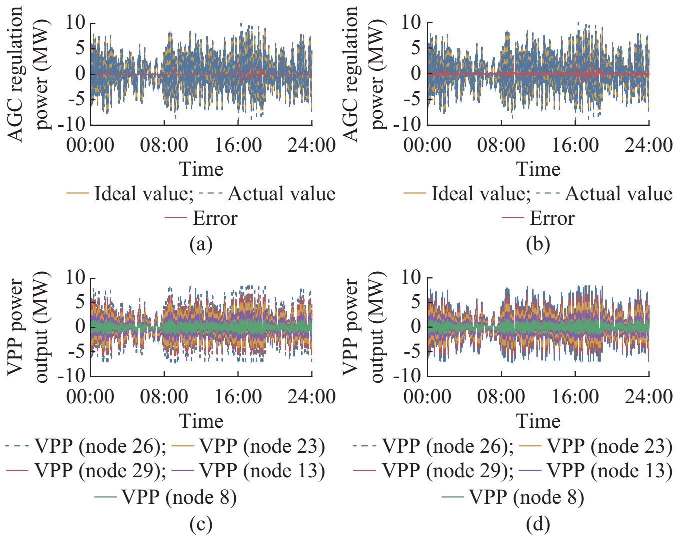

Fig. 10. AGC regulation power and VPP power output with different methods. (a) AGC regulation power with proposed power dispatch method. (b) AGC regulation power with Method 1. (c) VPP power output with proposed power dispatch method. (d) VPP power output with Method 1.

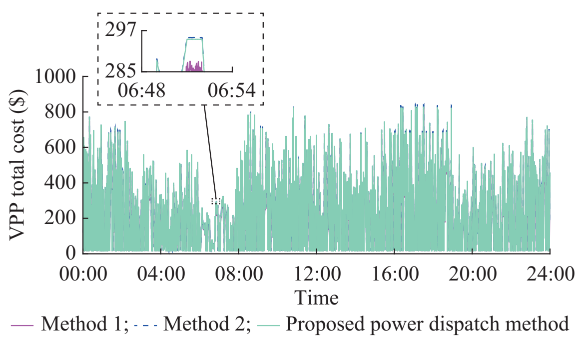

Fig. 11. Total cost of VPP with different methods.

TABLE III
PERFORMANCE COMPARISON RESULTS WITH DIFFERENT METHODS

Methods	Average power deviation (MW)	The maximum power deviation (MW)	Average total cost ($)
Method 1	0.0854	2.3437	234.67
Method 2	0.0057	2.0986	242.29
Proposed	0.0057	2.0986	241.69

B. Validity of Proposed Dynamic Power Regulation Control Method

To validate the effectiveness of the proposed dynamic power regulation control method, we examine the convergence performance of the ADAA in determining the optimal regulation power. Figure 12 presents the convergence process of ADDA for dynamic power regulation of each VPP in the AGC power regulation task ($P_0^{re} = 3.536$ MW) at time 14:41. As illustrated in Fig. 12, we can clearly observe that as the iteration number increases, the objective function, regulation power, and total cost of each VPP converges rapidly to the respective optimal values through the adjustment of step size. Therefore, the convergence performance and effectiveness of the proposed dynamic power regulation control method can be apparently validated according to the above convergence results.

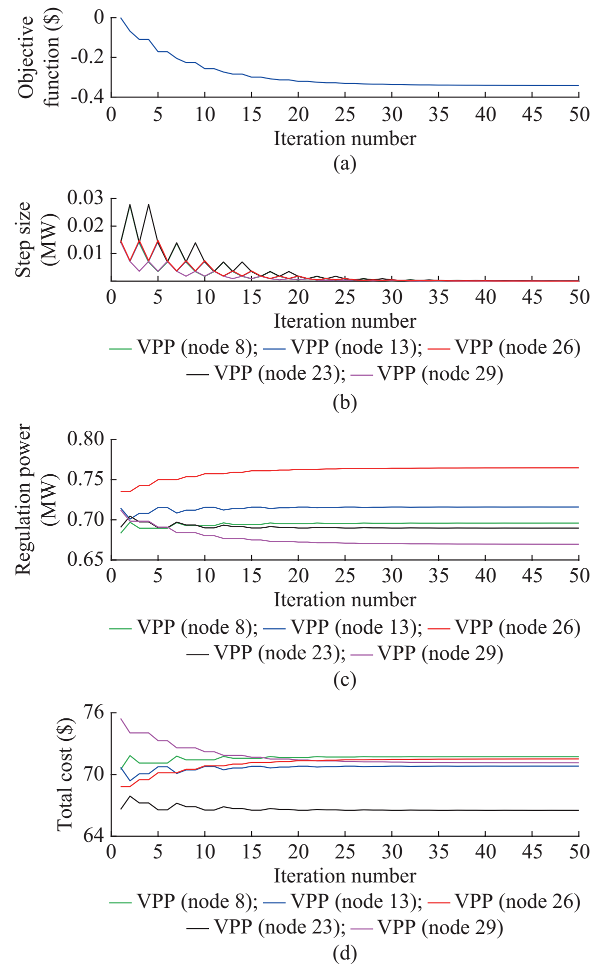

Fig. 12. Convergence process of ADDA for dynamic power regulation of each VPP. (a) Objective function. (b) Step size. (c) Regulation power. (d) Total cost.

To further illustrate the advantage of the proposed dynamic power regulation control method, the distributed auction-based method [26] is used for comparison. The convergence process of the total cost of VPPs with different methods at various time are compared in Fig. 13. We can find that both of these two methods can obtain the same optimal total costs within a finite number of iterations. However, the proposed dynamic power regulation control method can rapidly converge to the corresponding optimal values. Specifically, its convergence rate is approximately three times faster than that of the distributed auction-based method. This is because the proposed dynamic power regulation control method can adaptively adjust the exchange power by utilizing an adaptive swap size based solution, thereby determining the optimum faster. Hence, the advantage of the proposed dynamic power regulation control method can be clearly validated according to the simulation results.

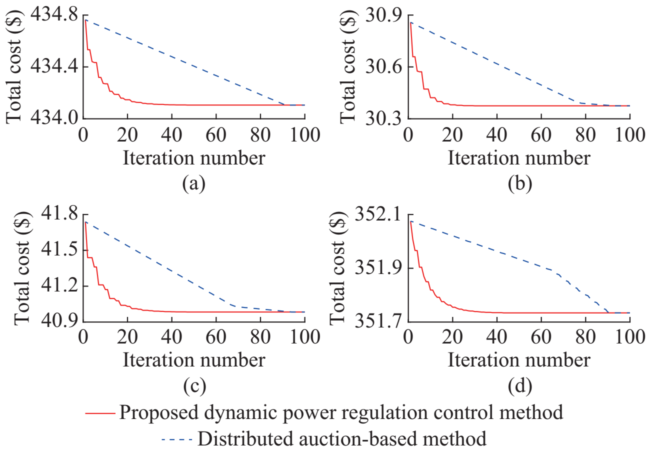

Fig. 13. Convergence process of total cost of VPP with different methods at various time. (a) 07:59. (b) 10:45. (c) 12:33. (d) 14:41.

VI. Conclusion

In this paper, we propose a novel co-design method of power dispatch with dynamic power regulation and communication transmission optimization under cloud-edge collaborations to achieve frequency control with VPPs. First, we develop a joint design scheme of power dispatch and routing optimization under cloud-edge collaborations. This scheme comprises a power dispatch method considering the influences of communication network, along with a routing optimization policy based on GCN. By adopting this scheme, we effectively mitigate the influences of communication network, thereby ensuring the accuracy and real-time performance of frequency control service. Furthermore, we present a dynamic power regulation strategy under edge-edge collaborations to determine the optimal regulation power for each VPP. This strategy significantly boosts the economic benefits of frequency control service through the application of the ADAA-based dynamic power regulation control method. Finally, the results illustrate that the proposed routing optimization policy reduces transmission delay by 21.61% and enhances network performance by 10.89%. Moreover, the joint design scheme decreases average power deviation by 93.33%. Besides, the proposed dynamic power regulation control method results in a notable decrease in average total cost by 0.25%, alongside a substantial enhancement in convergence speed, achieving an approximate increase of 66.67%. In conclusion, the simulation results verify the effectiveness and superiorities of the proposed co-design method for frequency control over some existing methods. In light of the inherent complexity of the actual communication environment, our future work will consider the impact of a hybrid communication environment on the frequency response performance of VPPs.

References

[1] X. Zhou, K. Strunz, T. Brown *et al.*, "Multi-energy system horizon planning: early decarbonisation in China avoids stranded assets," *Energy Internet*, vol. 1, no. 1, pp. 81-98, Aug. 2024.

[2] J. Li, Y. Qiao, Z. Lu *et al.*, "Integrated frequency-constrained scheduling considering coordination of frequency regulation capabilities from multi-source converters," *Journal of Modern Power Systems and Clean Energy*, vol. 12, no. 1, pp. 261-274, Jan. 2024.

[3] Q. Sun, J. Hu, R. Wang *et al.*, "Source-load cooperative frequency regulation based on virtual synchronous/asynchronous machine concept," *Energy Internet*, vol. 1, no. 2, pp. 188-199, Nov. 2024.

[4] J. Zhang, Z. Chen, N. Zhang *et al.*, "Frequency-constrained unit commitments with linear rules extracted from simulation results considering regulations from battery storage," *Journal of Modern Power Systems and Clean Energy*, vol. 11, no. 4, pp. 1041-1052, Jul. 2023.

[5] J. Guo, Y. Jing, W. Hou *et al.*, "Demands and challenges of energy storage technology for future power system," *Energy Internet*, vol. 1, no. 2, pp. 116-122, Nov. 2024.

[6] R. Zhang, B. Hredzak, and J. Fletcher, "Dynamic aggregation of energy storage systems into virtual power plants using distributed real-time clustering algorithm," *IEEE Transactions on Industrial Electronics*, vol. 68, no. 11, pp. 11002-11013, Nov. 2021.

[7] W. Bao, Q. Wu, L. Ding *et al.*, "A hierarchical inertial control scheme for multiple wind farms with BESSs based on ADMM," *IEEE Transactions on Sustainable Energy*, vol. 12, no. 2, pp. 751-760, Apr. 2021.

[8] X. Wang, L. Ying, K. Wen *et al.*, "Bi-level non-convex joint optimization model of energy storage in energy and primary frequency regulation markets," *International Journal of Electrical Power & Energy Systems*, vol. 134, p. 107408, Jan. 2022.

[9] Y. Arya, "AGC of PV-thermal and hydro-thermal power systems using CES and a new multi-stage FPIDF-(1+PI) controller," *Renewable Energy*, vol. 134, pp. 796-806, Apr. 2019.

[10] F. Zhang, Z. Hu, K. Meng *et al.*, "HESS sizing methodology for an existing thermal generator for the promotion of AGC response ability," *IEEE Transactions on Sustainable Energy*, vol. 11, no. 2, pp. 608-617, Apr. 2020.

[11] Y. Ma, Z. Hu, and Y. Song, "Hour-ahead optimization strategy for shared energy storage of renewable energy power stations to provide frequency regulation service," *IEEE Transactions on Sustainable Energy*, vol. 13, no. 4, pp. 2331-2342, Oct. 2022.

[12] J. Han, W. Lyu, H. Song *et al.*, "Optimization of communication network for distributed control of wind farm equipped with energy storages," *IEEE Transactions on Sustainable Energy*, vol. 14, no. 4, pp. 1933-1949, Oct. 2023.

[13] P. Kong, "Effects of communication network performance on dynamic pricing in smart power grid," *IEEE Systems Journal*, vol. 8, no. 2, pp. 533-541, Jun. 2014.

[14] P. Liu, K. Ma, J. Yang *et al.*, "Optimization of relay power and load control period based on cost-sharing contract in smart grid communications," *IEEE Internet of Things Journal*, vol. 8, no. 22, pp. 16559-16570, Nov. 2021.

[15] R. Ren, Y. Li, Q. Sun *et al.*, "Switched surplus-based distributed security dispatch for smart grid with persistent packet loss," *IEEE Internet of Things Journal*, vol. 11, no. 4, pp. 6185-6198, Feb. 2024.

[16] S. A. Hosseini, M. Fotuhi-Firuzabad, P. Dehghanian *et al.*, "Coordinating demand response and wind turbine controls for alleviating the first and second frequency dips in wind-integrated power grids," *IEEE Transactions on Industrial Informatics*, vol. 20, no. 2, pp. 2223-2233, Feb. 2024.

[17] J. Liang, S. Zeng, A. Li *et al.*, "A two-stage cloud edge collaborative regulation method for a distribution network considering the advance notification time of load," *Power System Protection and Control*, vol. 50, no. 23, pp. 121-132, Dec. 2023.

[18] K. Wang, J. Wu, X. Zheng *et al.*, "Cloud-edge orchestrated power dispatching for smart grid with distributed energy resources," *IEEE Transactions on Cloud Computing*, vol. 11, no. 2, pp. 1194-1203, Apr. 2023.

[19] Z. Zhang, Y. Zhang, D. Yue *et al.*, "Economic-driven hierarchical voltage regulation of incremental distribution networks: a cloud-edge collaboration based perspective," *IEEE Transactions on Industrial Informatics*, vol. 18, no. 3, pp. 1746-1757, Mar. 2022.

[20] D. Yue, Z. He, and C. Dou, "Cloud-edge collaboration-based distribution network reconfiguration for voltage preventive control," *IEEE Transactions on Industrial Informatics*, vol. 19, no. 12, pp. 11542-11552, Dec. 2023.

[21] D. Kreutz, F. M. V. Ramos, P. E. Veríssimo *et al.*, "Software-defined networking: a comprehensive survey," *Proceedings of the IEEE*, vol. 103, no. 1, pp. 14-76, Jan. 2015.

[22] H. Liu, H. Xie, H. Luo *et al.*, "Optimal strategy for participation of commercial HVAC systems in frequency regulation," *IEEE Internet of Things Journal*, vol. 8, no. 23, pp. 17100-17110, Dec. 2021.

[23] B. Liu and H. Wu, "Optimal planning and operation of hidden moving target defense for maximal detection effectiveness," *IEEE Transactions on Smart Grid*, vol. 12, no. 5, pp. 4447-4459, Sept. 2021.
[24] U. Maulik and S. Bandyopadhyay, "Performance evaluation of some clustering algorithms and validity indices," *IEEE Transactions on Pattern Analysis and Machine Intelligence*, vol. 24, no. 12, pp. 1650-1654, Dec. 2002.
[25] P. Lu, C. Jing, and X. Zhu, "GraphSAGE-based multi-path reliable routing algorithm for wireless mesh networks," *Processes*, vol. 11, no. 4, p. 1255, Apr. 2023.
[26] G. Binetti, A. Davoudi, D. Naso *et al*., "A distributed auction-based algorithm for the nonconvex economic dispatch problem," *IEEE Transactions on Industrial Informatics*, vol. 10, no. 2, pp. 1124-1132, May 2014.
[27] X. Zhang, T. Tan, B. Zhou *et al*., "Adaptive distributed auction-based algorithm for optimal mileage based AGC dispatch with high participation of renewable energy," *International Journal of Electrical Power & Energy Systems*, vol. 124, p. 106371, Jan. 2021.
[28] H. Shi, H. Feng, Z. Lu *et al*., "GRA-GCN: dense granule protein prediction in apicomplexa protozoa through graph convolutional network," *IEEE/ACM Transactions on Computational Biology and Bioinformatics*, vol. 20, no. 3, pp. 1963-1970, May 2023.
[29] T. K. Ho, "The random subspace method for constructing decision forests," *IEEE Transactions on Pattern Analysis and Machine Intelligence*, vol. 20, no. 8, pp. 832-844, Aug. 1998.
[30] Y. Wang, D. Sheng, H. Hu *et al*., "A novel series arc fault detection method based on Mel-frequency cepstral coefficients and fully connected neural network," *IEEE Access*, vol. 10, pp. 97983-97994, Sept. 2022.
[31] G. Camps-Valls and L. Bruzzone, "Kernel-based methods for hyperspectral image classification," *IEEE Transactions on Geoscience and Remote Sensing*, vol. 43, no. 6, pp. 1351-1362, Jun. 2005.
[32] S. Jia, J. Zhuang, L. Deng *et al*., "3-D Gaussian-Gabor feature extraction and selection for hyperspectral imagery classification," *IEEE Transactions on Geoscience and Remote Sensing*, vol. 57, no. 11, pp. 8813-8826, Nov. 2019.
[33] Q. Chen, L. Yang, D. Guo *et al*., "LEO satellite networks: when do all shortest distance paths belong to minimum hop path set?" *IEEE Transactions on Aerospace and Electronic Systems*, vol. 58, no. 4, pp. 3730-3734, Aug. 2022.
[34] S. Ragothaman, M. Maaref, and Z. M. Kassas, "Autonomous ground vehicle path planning in urban environments using GNSS and cellular signals reliability maps: models and algorithms," *IEEE Transactions on Aerospace and Electronic Systems*, vol. 57, no. 3, pp. 1562-1580, Jun. 2021.
[35] K. Ko and D. K. Sung, "The effect of cellular network-based communication delays in an EV aggregator's domain on frequency regulation service," *IEEE Transactions on Smart Grid*, vol. 10, no. 1, pp. 65-73, Jan. 2019.

Jinrui Guo received the M.S. degree in electrical engineering from Nanjing University of Posts and Telecommunications, Nanjing, China, in 2023. He is currently pursuing the Ph.D. degree in control science and engineering with Nanjing University of Posts and Telecommunications. His current research interest includes cyber-physical power system.

Chunxia Dou received the B. S. and M. S. degrees in automation from Northeast Heavy Machinery Institute, Qiqihaer, China, in 1989 and 1994, respectively, and the Ph. D. degree in control theory and control engineering from the Institute of Electrical Engineering, Yanshan University, Qinhuangdao, China, in 2005. In 2010, she joined the Department of Engineering, Peking University, Beijing, China, where she was a Postdoctoral Fellow for two years. Since 2015, she has been a Professor with the Institute of Advanced Technology for Carbon Neutrality, Nanjing University of Posts and Telecommunications, Nanjing, China. Her current research interests include multiagent based control, distributed coordinated control, and their applications in power system and smart grid.

Dong Yue received the Ph. D. degree from the South China University of Technology, Guangzhou, China, in 1995. He is currently a Professor and the Dean with the Institute of Advanced Technology for Carbon Neutrality, Nanjing University of Posts and Telecommunications, Nanjing, China, and also a Changjiang Professor with the Department of Control Science and Engineering, Huazhong University of Science and Technology, Wuhan, China. His current research interests include analysis and synthesis of networked control system, multiagent system, optimal control of power system, and Internet of Things.

Zhijun Zhang received the Ph.D. degree in information acquisition and control from the Nanjing University of Posts and Telecommunications, Nanjing, China, in 2022. He is currently a Postdoctoral Fellow with the City University of Hong Kong, Hong Kong, China. From 2023 to 2025, he was a Research Fellow with School of Electrical and Electronic Engineering, Nanyang Technological University, Singapore. His current research interests include optimal operation of power system, energy storage system, and electric vehicle.

Zhanqiang Zhang received the first B. S. degree in electrical engineering and automation and the second B.S. degree in math and applied mathematics from the Hebei University of Science and Technology, Shijiazhuang, China, in 2015, and the Ph. D. degree in control science and engineering from Yanshan University, Qinhuangdao, China, in 2021. He was a Visiting Ph.D. Student with the Queensland University of Technology, Brisbane, Australia, from 2019 to 2020. He is currently a Research Associate with the Institute of Advanced Technology for Carbon Neutrality, Nanjing University of Posts and Telecommunications, Nanjing, China. His research interests include microgrid and active distribution network.

Bo Zhang received the Ph. D. degree from Yanshan University, Qinhuangdao, China, in 2022. He is currently a Lecturer with the Institute of Advanced Technology for Carbon Neutrality, Nanjing University of Posts and Telecommunications, Nanjing, China. His current research interests include microgrid and distribution network.